1 **An *in vitro* tumorigenesis model based on live cell-generated oxygen and nutrient gradients**

2 Anne C. Gilmore[1][§], Sarah J. Flaherty[1], Veena Somasundaram[2], David A. Scheiblin[3], Stephen J.

3 Lockett[3], David A. Wink[2], William F. Heinz[3*]

4

5 [1]Optical Microscopy and Analysis Laboratory, Office of Science and Technology Resources, Center

6 for Cancer Research, National Cancer Institute, National Institutes of Health

7 [2]Laboratory of Cancer Immunometabolism, Center for Cancer Research, National Cancer

8 Institute, National Institutes of Health

9 [3]Optical Microscopy and Analysis Laboratory, Cancer Research Technology Program, Frederick

10 National Laboratory for Cancer Research, Frederick, MD

11 [§]Current address: Graduate School of Biomedical Sciences, St. Jude Children's Research Hospital,

12 Memphis, TN.

13

14 *Running title*: Oxygen and nutrient gradient tumorigenesis model

15 *Keywords*: hypoxia, tumor microenvironment, live cell model

16 *Correspondence should be addressed to*:

17 William F. Heinz
18 Optical Microscopy and Analysis Laboratory
19 Frederick National Lab For Cancer Research
20 Leidos Biomedical Research, Inc.
21 P.O. Box B
22 Frederick, MD 21702
23 301-846-1239
24 Will.heinz@nih.gov
25

An *in vitro* tumorigenesis model based on live cell-generated oxygen and nutrient gradients. Gilmore, et al., 2020.

26   **The tumor microenvironment (TME) is multi-cellular, spatially heterogenous, and contains**

27   **cell-generated gradients of soluble molecules. Current cell-based model systems lack this**

28   **complexity or are difficult to interrogate microscopically. We present a 2D live-cell chamber**

29   **that approximates the TME and demonstrate that breast cancer cells and macrophages**

30   **generate hypoxic and nutrient gradients, self-organize, and have spatially varying phenotypes**

31   **along the gradients, leading to new insights into tumorigenesis.**

32

33   Concentration gradients of soluble molecules in tissue are established by their release

34   from and consumption by cells in combination with extracellular diffusion. These gradients

35   influence the spatial organization and phenotypes of cells in solid tissues, including tumors[1].

36   Current experimental tissue models do not capture the complex spatial organization of

37   cells and molecules, and they can be difficult to interrogate microscopically. Standard 2D cell

38   culture does not replicate long-range (> 100 µm) gradients of extracellular molecules within the

39   TME. Microfluidic systems can impose diffusive gradients on 2D cell cultures and are designed

40   for microscopic interrogation[2, 3], but they control only a limited number of molecules of

41   interest, the spatial organization of cells is not the same as tissue, and the molecular gradients

42   are not naturally cell driven. Although organoids and spheroids reflect to some extent the

43   molecular gradients that arise in actual tissues, they vary in structure[4] and are challenging to

44   examine and quantify at high spatial resolution with long term live-cell microscopy[5].

45   Hypoxic gradients in 2D cell culture were observed in 2018 in restricted exchange

46   environment chambers (REECs)[6]. Cells in this chamber, supported on a standard #1.5 glass

47   coverslip (0.17 mm thick), grow in a small (< 20 µL) lower compartment separated from a larger
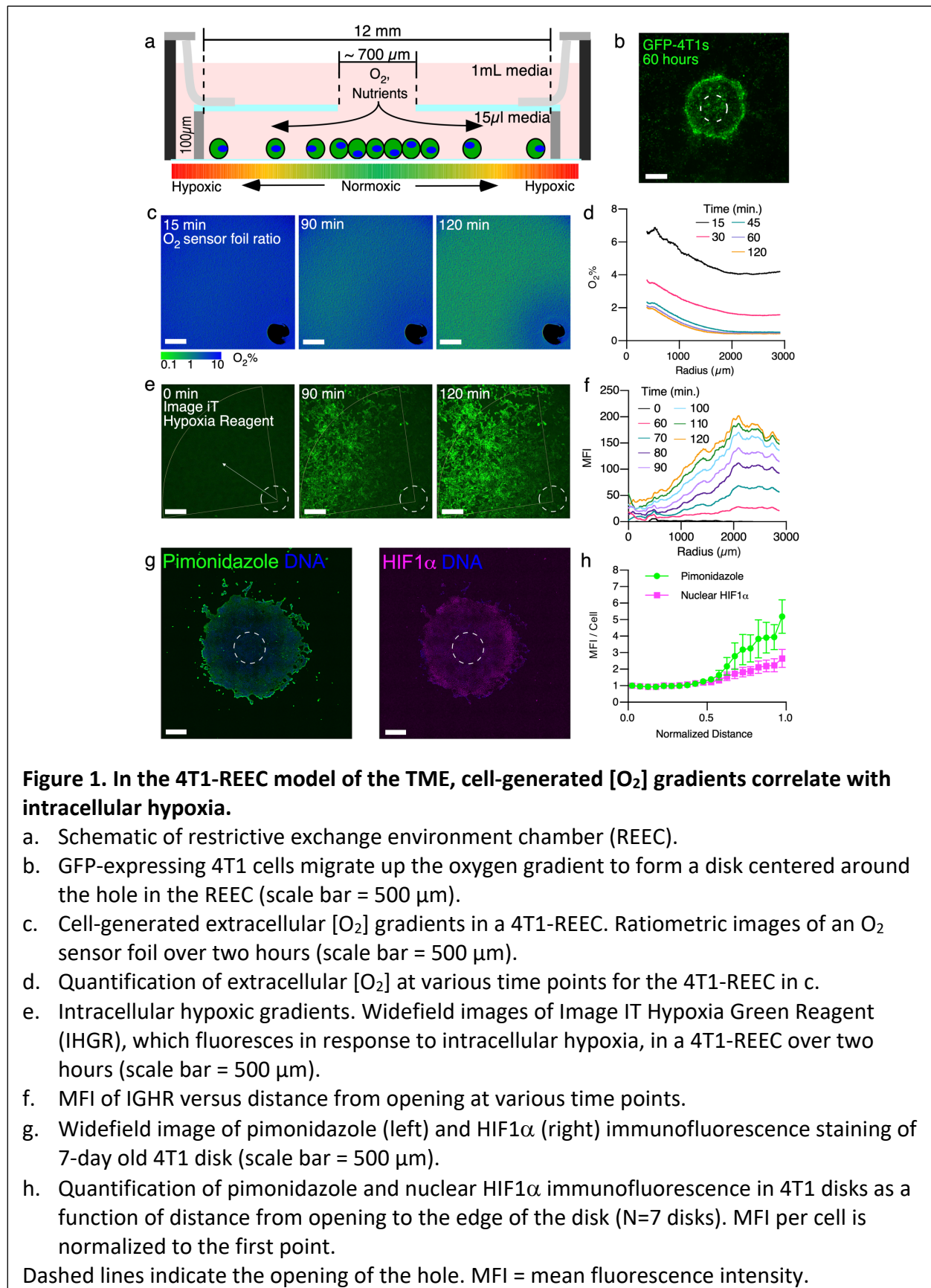
48   upper compartment (~ 1 mL) by a coverslip with a small central hole (~0.7 mm diameter)

49   through which O_2 and soluble molecules (e.g., nutrients, cytokines, and cellular waste products)

50   diffuse between the compartments (Fig. 1a). Thus, cells directly beneath the hole are exposed

51   to O_2 and nutrients at the concentration of the upper compartment, while cells distal to the

52   hole exist in a cell-generated hypoxic environment.

53   Here we report the application of the chamber to investigate the TME. Specifically, we

54   examine the role of O_2 and nutrient gradients on tumor and immune cell phenotype, using 4T1

55   mouse mammary tumor cells and ANA-1 mouse macrophages as exemplars. The 4T1 model

56   shares many features with triple negative human breast cancer[7], and macrophages are the

57   most abundant non-cancer cells in the TME and play an immunosuppressive role in

58   tumorigenesis[8]. These cells types were cultured separately and in co-culture in the chamber,

59   and the spatiotemporal dynamics of O_2 gradient formation, nutrient uptake, cell migration and

60   cell survival were quantified.

Results

62   GFP-tagged 4T1 cells, initially uniformly distributed (~75% confluence) in the lower

63   compartment, began migrating towards the hole within 36 h and formed a stable disk with a

64   diameter of ~1 mm within ~60 h (Fig. 1b, Supplemental Video 1). Beyond the disk, cells

65   detached from the bottom of the well and died (Supplementary Fig. 1), analogous to necrotic

66   zones in solid tumors. The resulting 4T1-disk remained alive and stable for at least three weeks

67   with periodic changes to media in the upper compartment. We attribute the directed motion of

68   cells to O_2 gradients within the chamber, which do not arise in standard cell culture and cannot

69   be readily observed in intact tumors or 3D cell culture models. 4T1 proliferation recovers with

An *in vitro* tumorigenesis model based on live cell-generated oxygen and nutrient gradients. Gilmore, et al., 2020.

Figure 1. In the 4T1-REEC model of the TME, cell-generated [O₂] gradients correlate with intracellular hypoxia.

a. Schematic of restrictive exchange environment chamber (REEC).

b. GFP-expressing 4T1 cells migrate up the oxygen gradient to form a disk centered around the hole in the REEC (scale bar = 500 μm).

c. Cell-generated extracellular [O₂] gradients in a 4T1-REEC. Ratiometric images of an O₂ sensor foil over two hours (scale bar = 500 μm).

d. Quantification of extracellular [O₂] at various time points for the 4T1-REEC in c.

e. Intracellular hypoxic gradients. Widefield images of Image IT Hypoxia Green Reagent (IHGR), which fluoresces in response to intracellular hypoxia, in a 4T1-REEC over two hours (scale bar = 500 μm).

f. MFI of IGHR versus distance from opening at various time points.

g. Widefield image of pimonidazole (left) and HIF1α (right) immunofluorescence staining of 7-day old 4T1 disk (scale bar = 500 μm).

h. Quantification of pimonidazole and nuclear HIF1α immunofluorescence in 4T1 disks as a function of distance from opening to the edge of the disk (N=7 disks). MFI per cell is normalized to the first point.

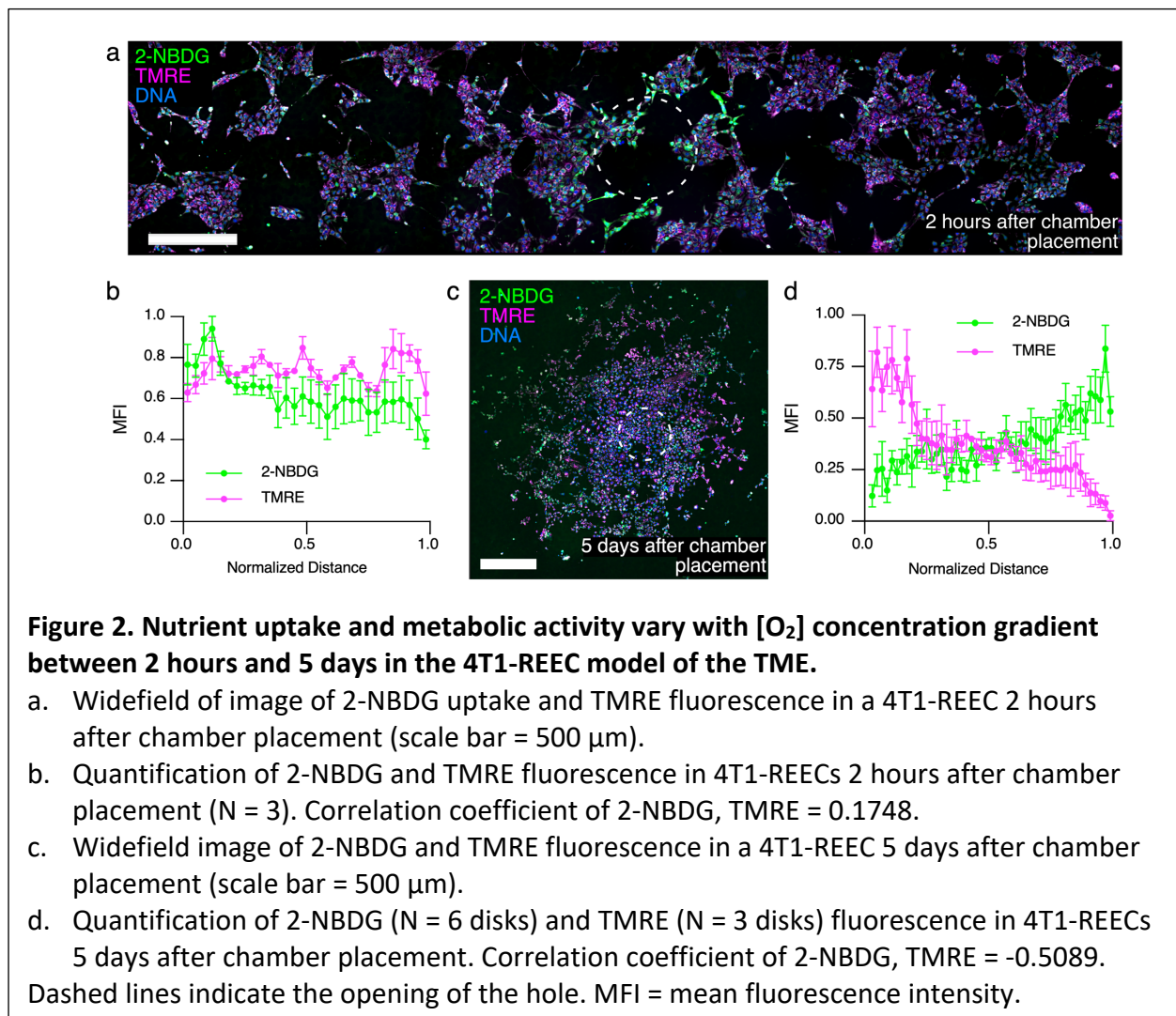Dashed lines indicate the opening of the hole. MFI = mean fluorescence intensity.

70

71   disk expansion after the chamber is removed (Supplemental Fig. 2) and normoxia is

72   reestablished. Interestingly, this experiment showed that 4T1 cells could respond to the

73   gradient of O_2 by converting to a migratory phenotype in order to coalesce near the opening in

74   the chamber. This behavior is characteristic of tumor cells *in vivo* and was shown here to be

75   possible without the presence of other cell types, extracellular matrix, or 3D environment.

76   After demonstrating that REECs reproduce tumor behavior, we quantitatively

77   characterized the hypoxia and nutrient gradients, and how these gradients affected 4T1

78   phenotype and metabolism. Dissolved extracellular O_2 concentration ($[O_2]$) measurements in

79   the REECs showed that stable radial negative gradients formed rapidly (< 2 h) after chamber

80   placement onto uniformly distributed 4T1 cells in 2D cell culture (Fig. 1c, d; Supplemental Fig.

81   3), which agreed with mathematical modeling (Supplemental Fig. 4). Fluorescence labeling of

82   the live 4T1 cells with the image-iT green hypoxia reagent (IGHR) revealed that positive

83   gradients of intracellular hypoxia formed in a similar timescale, and the hypoxic front (the

84   distance at which the IGHR signal is 90% of its maximum) was within a millimeter of the edge of

85   the opening after 2 h (Fig. 1e, f).

86   Hypoxia, through hypoxia inducible factor (HIF1α) stabilization, can induce pro-tumor

87   phenotypes (Supplemental Fig. 5), including a collective-to-amoeboid transition, increased in

88   vimentin expression, and migration of 4T1 cells[9]. Cells in the periphery of the disks exhibit a

89   temporary increase in vimentin expression relative to E-cadherin expression, between 12 and

90   36 hours after initiation, suggesting a transient phenotypic shift to a mesenchymal state

91   (Supplemental Fig. 6)[10]. In stable disks, increased cellular hypoxia distal to the hole was

92   measured by pimonidazole reduction and HIF1α localization to the nuclei (Fig. 1g, h).

An *in vitro* tumorigenesis model based on live cell-generated oxygen and nutrient gradients. Gilmore, et al., 2020.

93   During initial O_2 gradient formation (< 2 h) glucose consumption exhibited a radial

94   gradient with maximum consumption at the opening at early time points (Fig. 2a, b;). However,

95   no gradient of mitochondrial membrane potential ($\Delta\Psi$m) was observed via

96   tetramethylrhodamine-ethyl-ester (TMRE) fluorescence 2 hours after chamber placement,

97   suggesting that oxidative phosphorylation continues for some time after hypoxia is established.

98   In fully formed disks (> 72 h), $\Delta\Psi$m decreased while glucose consumption increased with radial

99   distance (Fig. 2c, d, Supplemental Fig. 7), consistent with a metabolic shift from oxidative

100   phosphorylation to glycolysis in the hypoxic region. Mathematical modeling predicted no

Figure 2. Nutrient uptake and metabolic activity vary with [O₂] concentration gradient between 2 hours and 5 days in the 4T1-REEC model of the TME.

a. Widefield of image of 2-NBDG uptake and TMRE fluorescence in a 4T1-REEC 2 hours after chamber placement (scale bar = 500 μm).
b. Quantification of 2-NBDG and TMRE fluorescence in 4T1-REECs 2 hours after chamber placement (N = 3). Correlation coefficient of 2-NBDG, TMRE = 0.1748.
c. Widefield image of 2-NBDG and TMRE fluorescence in a 4T1-REEC 5 days after chamber placement (scale bar = 500 μm).
d. Quantification of 2-NBDG (N = 6 disks) and TMRE (N = 3 disks) fluorescence in 4T1-REECs 5 days after chamber placement. Correlation coefficient of 2-NBDG, TMRE = -0.5089.
Dashed lines indicate the opening of the hole. MFI = mean fluorescence intensity.
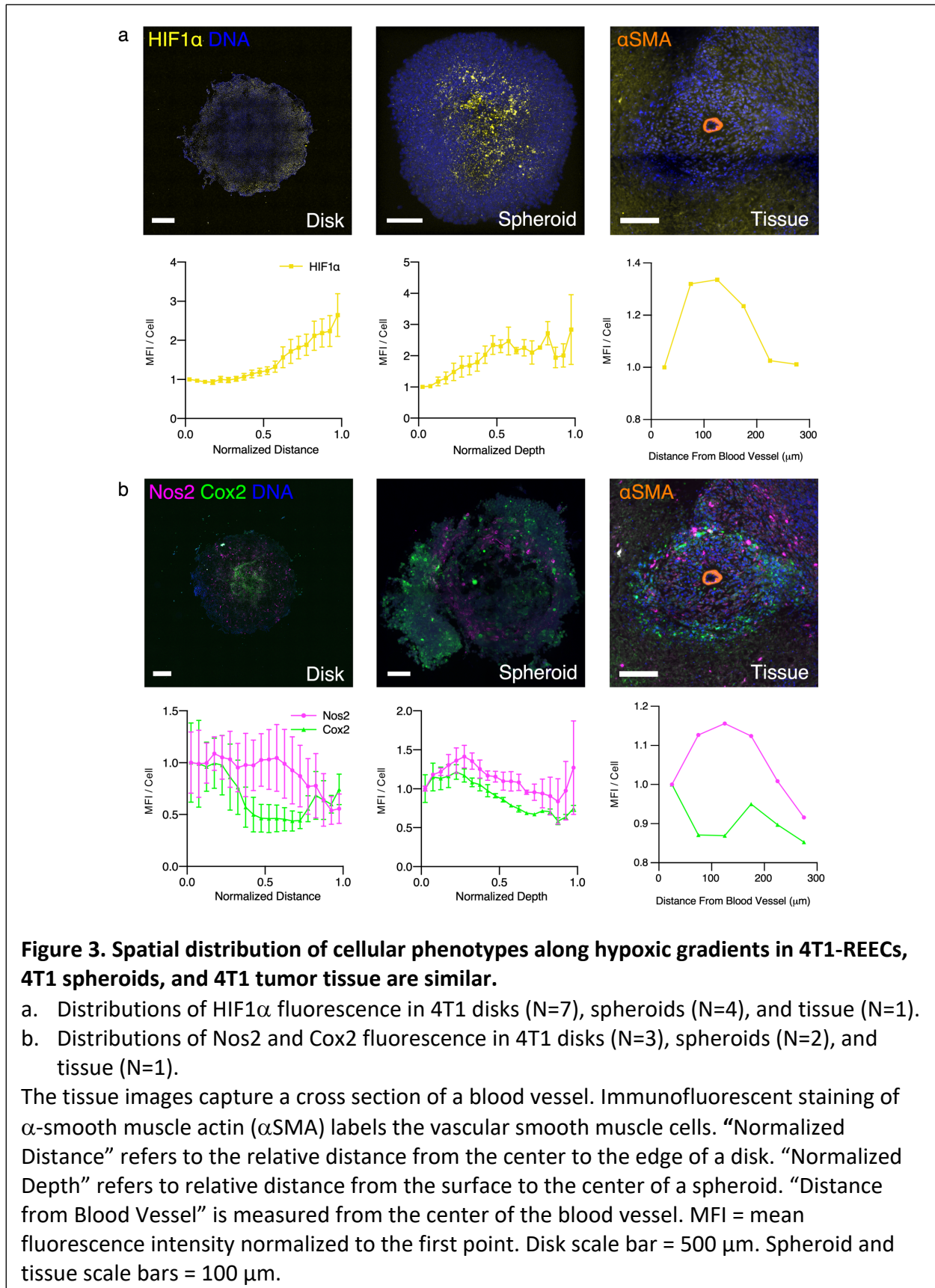
6

An *in vitro* tumorigenesis model based on live cell-generated oxygen and nutrient gradients. Gilmore, et al., 2020.

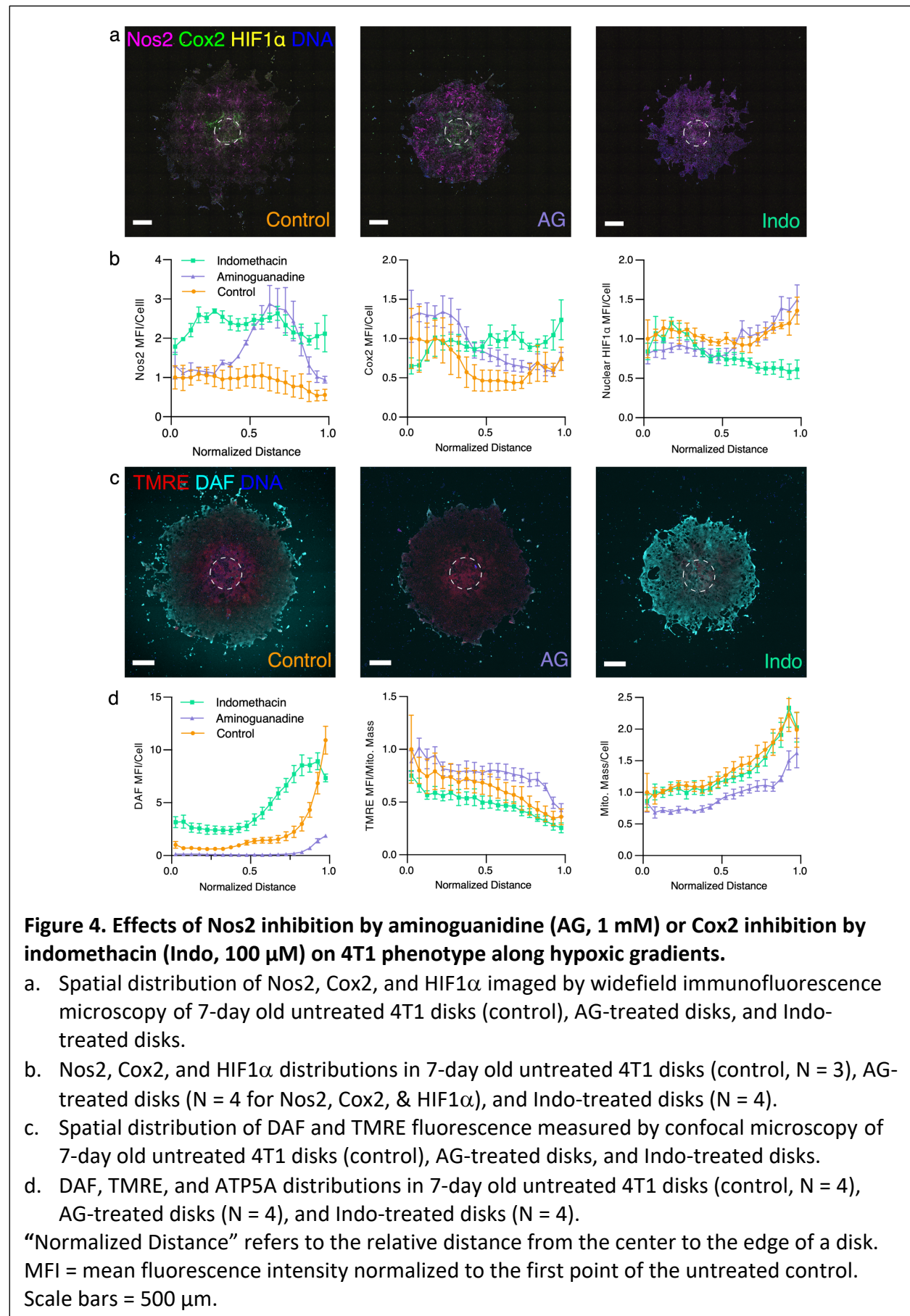101   significant gradient of glucose in the media away from the standard serum glucose

102   concentration (22.5 mM), which is far in excess of the metabolic needs of the cells

103   (Supplemental Fig. 4). Thus, we conclude the [O_2] gradient alone drove the metabolic shift.

104   These results demonstrate that REECs capture key features of hypoxia and metabolism in 4T1

105   tumorigenesis.

106   We utilized REECs to further understand the immunosuppressive role of the

107   inflammatory proteins inducible nitric oxide synthase (Nos2) and cyclooxygenase-2 (Cox2) in

108   the tumorigenic microenvironment. Clinically, high expression of both these proteins in ER-

109   human breast cancer is an indicator of very poor prognosis[11]; both are potential targets for

110   therapy using FDA-approved anti-inflammatory drugs in combination with standard treatments.

111   Nos2 produces nitric oxide (NO), a key regulator of cancer processes[12], from L-arginine and is

112   upregulated by stabilized HIF1α in response to hypoxia and nutrient deprivation[13]

113   (Supplemental Fig. 5). Therefore, we postulated that in the hypoxic regions of fully formed

114   disks, the Nos2 expression and NO flux would be high relative to Cox2-expression. We observed

115   Nos2 levels remain high relative to Cox2 in the hypoxic regions of disks, spheroids, and tissue

116   (Fig. 3a, b, Supplemental 8). We also saw a large increase in NO flux in the hypoxic regions of

117   4T1-disks, confirming our hypothesis (Figure 4a-d, control disks; Supplemental 8).

118   We observed in disks, spheroids, and tumor tissue that different 4T1 cells expressed

119   high levels of Nos2 or Cox2 and that high Nos2-expressing cells tended to be clustered together

120   (Fig. 3b, Supplemental Fig. 9) under hypoxia-induced stress conditions. The fact that Nos2 and

121   Cox2 are highly expressed in different cells indicates that these proteins likely drive the

122   expression and activity of each other via an intercellular feed-forward mechanism[14] mediated

7

Figure 3. Spatial distribution of cellular phenotypes along hypoxic gradients in 4T1-REECs, 4T1 spheroids, and 4T1 tumor tissue are similar.

a. Distributions of HIF1α fluorescence in 4T1 disks (N=7), spheroids (N=4), and tissue (N=1).
b. Distributions of Nos2 and Cox2 fluorescence in 4T1 disks (N=3), spheroids (N=2), and tissue (N=1).

The tissue images capture a cross section of a blood vessel. Immunofluorescent staining of α-smooth muscle actin (αSMA) labels the vascular smooth muscle cells. "Normalized Distance" refers to the relative distance from the center to the edge of a disk. "Normalized Depth" refers to relative distance from the surface to the center of a spheroid. "Distance from Blood Vessel" is measured from the center of the blood vessel. MFI = mean fluorescence intensity normalized to the first point. Disk scale bar = 500 µm. Spheroid and tissue scale bars = 100 µm.

123

124   by the release of NO and PGE2 from the cells[11]. Nos2-expressing cell clumps likely lead to

125   significantly higher local concentrations of NO than could arise when Nos2-expressing cells are

126   scattered and isolated[15] and thus augment this paracrine mechanism.

127   Inhibitors of Nos2 and Cox2 interrupt the feed-forward loop and reduce tumor growth

128   rate[11, 13]. We therefore treated 4T1 disks in REECs with Nos2 or Cox2 inhibitors for 7 days to

129   examine the effect of the inhibitors on the distribution of protein expression, NO release,

130    $\Delta\Psi$m, and mitochondrial mass within the disks (Fig. 4a-d).

131   Treatment with the Nos2 inhibitor aminoguanidine (AG, 1 mM) resulted in a large

132   compensatory increase in Nos2 expression in the more hypoxic regions of the disk versus the

133   untreated control, minimal NO levels, as well as increased Cox2 expression in the more

134   normoxic regions of the disk. Treatment with the Cox inhibitor indomethacin (Indo, 100 μM)

135   likewise resulted in a compensatory increase in Cox2 expression in hypoxic regions of the disk

136   and increased Nos2 expression and NO levels across the disk relative to control. Interestingly,

137   nuclear HIF1α levels were lower in the hypoxic regions of Indo-treated disks relative to the

138   controls (Fig. 4a, b). Given that NO flux increases in the hypoxic region with indomethacin

139   treatment (Fig. 4c, d), this is most likely due to the known inhibitory effect of NO on HIF1α in

140   hypoxic conditions[16].

141        $\Delta\Psi$m was higher in more normoxic regions compared to hypoxic regions for both

142   treatments and controls, as expected (Fig. 4c, d). Relative to controls, $\Delta\Psi$m was lower in Indo-

143   treated disks, indicating decreased mitochondrial activity in response to the higher levels of NO

144   across the disk, as expected. $\Delta\Psi$m was higher in AG treated disks, particularly in the hypoxic

145   regions, indicating a failure to switch to anaerobic metabolism in absence of functional Nos2.

An *in vitro* tumorigenesis model based on live cell-generated oxygen and nutrient gradients. Gilmore, et al., 2020.

Figure 4. Effects of Nos2 inhibition by aminoguanidine (AG, 1 mM) or Cox2 inhibition by indomethacin (Indo, 100 μM) on 4T1 phenotype along hypoxic gradients.

a. Spatial distribution of Nos2, Cox2, and HIF1α imaged by widefield immunofluorescence microscopy of 7-day old untreated 4T1 disks (control), AG-treated disks, and Indo-treated disks.

b. Nos2, Cox2, and HIF1α distributions in 7-day old untreated 4T1 disks (control, N = 3), AG-treated disks (N = 4 for Nos2, Cox2, & HIF1α), and Indo-treated disks (N = 4).

c. Spatial distribution of DAF and TMRE fluorescence measured by confocal microscopy of 7-day old untreated 4T1 disks (control), AG-treated disks, and Indo-treated disks.

d. DAF, TMRE, and ATP5A distributions in 7-day old untreated 4T1 disks (control, N = 4), AG-treated disks (N = 4), and Indo-treated disks (N = 4).

"Normalized Distance" refers to the relative distance from the center to the edge of a disk.

MFI = mean fluorescence intensity normalized to the first point of the untreated control.

Scale bars = 500 μm.

146

147   Additionally, mitochondrial mass was lower in the AG treated disks (Fig. 4d), likely due to the

148   lack of NO, which plays an important role in mitochondrial biogenesis[17]. Indo-treated 4T1 disks

149   contained fewer cells than control disks, mirroring effects of the anti-inflammatories in tumors

150   (Supplementary Fig. 10)[12,13]. These results show that anti-inflammatory compounds modulate

151   cellular phenotypes along the hypoxic gradient, which demonstrates the utility of the 4T1-REEC

152   system for understanding treatment mechanisms in conjunction with hypoxia in the TME.

153   Macrophages localize to areas of hypoxia and necrosis in the TME where they play an

154   immunosuppressive role[18]. Therefore, we cultured ANA-1 macrophages in the REEC either

155   alone or with 4T1 cells. The macrophages, unlike 4T1 cells did not migrate towards the opening

156   or form disks, though they did generate a hypoxic gradient as observed via IGHR staining

157   (Supplemental Fig. 11). Macrophages treated with the pro-inflammatory cytokines IFNγ and LPS

158   express higher levels of Nos2 and thus produce more NO, which converts them to a glycolytic

159   pathway and decreases their mitochondrial metabolism and O_2 consumption[15]. This effect was

160   observed in REECs as the hypoxic front of treated macrophages was further from the hole than

161   that of untreated cells (Supplemental Fig. 11). When macrophages were co-cultured with 4T1s

162   or injected through the hole onto stable 4T1 disks, the macrophages populated the hypoxic and

163   4T1-necrotic regions (Supplemental Fig. 11). These results are consistent with macrophage

164   behavior in spheroids and *in vivo* in which IFNγ+LPS stimulated macrophages infiltrate the

165   hypoxic core of spheroids (Supplemental Fig. 12) and hypoxic regions of tumors[19]. Interestingly,

166   the area of stable 4T1 disks decreased following the injection of unstimulated macrophages.

167   Injection of stimulated macrophages or fresh media resulted in increases in 4T1 disk area

168   (Supplemental Figure 11). This suggests that the stimulated macrophage-generated increase in

169   extracellular NO in the chamber drives glycolysis and reduces the O_2 consumption of the 4T1

170   and ANA1 cells enough to push back the hypoxic front, thereby promoting survival and

171   proliferation of the tumor cells.

172   In conclusion, we demonstrated that the 4T1/ANA1-REEC *in vitro* model captures key

173   features of the tumorigenic microenvironment. It recapitulates the cell-generated oxygen

174   gradients that exist in solid tumors and via live-cell microscopy can reveal cell dynamics and

175   phenotypes that cannot be readily determined from actual tumors. Hence, the REEC system is a

176   powerful tool to investigate mechanisms of tumorigenesis, immunotherapy, and anti-

177   inflammatory treatments in live cells in a tumor-like environment.

An *in vitro* tumorigenesis model based on live cell-generated oxygen and nutrient gradients. Gilmore, et al., 2020.

Methods

178

179 **REEC design and assembly**

180 The REECs design was modified to improve functionality and fit 12-well glass-bottom plates

181 (Figure 1A). For each REEC, a through hole (~700 µm diameter) was manually machined into a

182 circular cover glass (18 mm diameter) using a high-speed air drill and tapered carbide bit (SCM

183 Systems, Inc, Menomonee Falls, WI). A stainless-steel O-ring (0.100 mm thick, 12 mm ID, 18 mm

184 OD) was epoxied to one side of the cover glass using UV-curable epoxy (Norland Products, Inc.).

185 Laser-machined mylar clamps were epoxied to the other side of the cover glass using the same

186 epoxy. Between each step, the epoxy was cured for 5 minutes in a UV-Ozone cleaner (Model

187 342, Jelight). Chambers were UV-sterilized immediately prior to use in cell culture

188 (Supplemental Protocol).

189

190 The stainless-steel O-ring has as smoother, more uniform contact surface compared to the

191 laser-machined Mylar gasket that was used in previously published studies. The epoxy layer

192 between the steel spacer and the cover glass adds approximately 40 µm to the height of the

193 chamber. Average chamber height was 138.4 µm +/- 12.1 µm, and the interior volume was

194 approximately 15.65 µL. The average hole diameter was 740.1 +/- 125.1 µm.

195

196 **Cell culture and plating for the REEC/4T1 system**

197 Murine mammary triple negative breast cancer 4T1 cells were cultured in complete media

198 (DMEM media, 25 mM glucose, 10% fetal bovine serum (FBS), penicillin, and streptomycin;

An *in vitro* tumorigenesis model based on live cell-generated oxygen and nutrient gradients. Gilmore, et al., 2020.

199   Quality Biologicals). GFP-expressing 4T1 cells, 4T1-Fluc-Neo/eGFP-Puro cells (GFP-4T1, Imanis

200   Life Sciences), were grown in complete media and selected for using G418 and puromycin. Prior

201   to plating, laser-machined Mylar rims were epoxied on to a 12 well-plate. The Mylar rims

202   ensure that the Mylar clamps of each REEC are able to firmly hold the REEC against the bottom

203   of the well. 4T1 cells were then plated (200,000 cells/mL, 1 mL/well) and incubated at 37°C.

204   Once the 4T1 cells reached 70-80% confluency (~24 hours), the media was refreshed and REECs

205   were placed with sterilized forceps and pressed firmly to the bottom of the well. Media in the

206   upper chamber was refreshed every 3-4 days with the least possible disturbance to the lower

207   chamber possible.

208

209   **Mathematical model**

210   The REEC/4T1 system was simulated as an annulus containing a uniform density of consumers

211   and used a diffusion-consumption model[20] to characterize the time-evolution and steady state

212   behavior of oxygen and glucose. For a radially symmetric system, the concentration (C) of a

213   molecular species is described by

214
$$\frac{\partial C}{\partial t} = \frac{1}{r}\frac{\partial}{\partial r}\left(rD\frac{\partial C}{\partial r}\right) - n_{consumers}k_{consumption}f(C)$$

215   Where n = concentration of consumers, k = the per-cell consumption rate, and $f(C)$ is a function

216   of concentration and can be written as

217
$$f(C) = C_{bulk}\frac{1}{1+\frac{C_{bulk}}{C}}$$

218   At steady state, a characteristic distance can be defined as

14

An *in vitro* tumorigenesis model based on live cell-generated oxygen and nutrient gradients. Gilmore, et al., 2020.

219
$$\lambda = \sqrt{\frac{D}{n \cdot k}}$$

220   k, can be calculated from the maximum per cell molecular consumption rate, A_{max}, and the

221   concentration of the molecule of interest, C_{bulk}

222
$$A_{max} = kC_{bulk}$$

223

224   MATLAB's partial differential equation toolbox was used to model the evolution of

225   oxygen and glucose gradients within the REEC/4T1 system at 37 °C. The system was defined as

226   an annulus with an inner radius, r_1, of 350 μm and an outer radius, r_2, of 6,000 μm,

227   corresponding to the radius of the REEC opening and the inner radius of the REEC, respectively.

228   The inner radius was modeled as a source of the diffusing molecules with a constant

229   concentration, C_{bulk}.

230   Thus, the boundary conditions were

231
$$C(r_1, t) = C_{bulk}$$

232
$$\frac{\partial C(r_2, t)}{\partial r} = 0$$

233   The initial condition corresponded to the moment the chamber was placed in the well:

234
$$C(r, 0) = C_{bulk}$$

235   Oxygen diffusion, glucose diffusion, and glucose consumption rate values for 4T1 cells were

236   based on the literature[23-27]. Oxygen consumption rate (OCR) was measured directly via a

237   Seahorse XF96 metabolic analyzer (see below).

238

239

An *in vitro* tumorigenesis model based on live cell-generated oxygen and nutrient gradients. Gilmore, et al., 2020.

240   Table 1.

Parameter	Value	Reference
D ($\mu m^2/s$)		
O_2	3,370	21
Glucose	616	22
Amax (molecules/cell/s)		
O_2	2.98×10^7	OCR measured with Seahorse XF mito-stress test with 4T1 cells.
Glucose	6.47×10^7	23
C_{bulk}		
O_2	178 μM, 171 μM	24, 25
Glucose	25 mM	DMEM media specification (Quality Biologicals)

241

242   The oxygen concentration used in the dynamic model at $r < 350$ μm is 171 μM, not 178 μM

243   which is the value at the interface of the media and the atmosphere. It is somewhat less

244   because the cells immediately below the opening in the REEC consume the oxygen diffusing

245   through the opening in the coverglass. To account for this, we modeled the oxygen

246   concentration in a column of media 250 μm tall (100 μm high REEC and a 150 μm thick

247   coverglass) above a monolayer of 4T1 cells using a model based on Fick's law[25]. At the top of

248   the column, the media above the REEC coverglass is assumed to be fully oxygenated (178 μM).

249   Using a 4T1 density was 200,000 cells/cm^2 and the Amax for the 4T1s, the O_2 concentration at

250   the cell layer was calculated to be 171 μM.

251

252   For each molecular species, the simulation was run for an equivalent of 48 hours for each

253   combination of maximum cellular molecular consumption rate, A_{max}, and cell density, *n*.

254   Convergence to steady state was defined as a change in RMS difference of less than 0.1 %

255   between successive profiles.

256

Oxygen consumption rate measurements

258   4T1 cells' OCR was measured using the XF96 Seahorse Metabolic Analyzer (Agilent

259   Technologies, California). 4T1s were plated (1×10^5 cells) in each well (200 µL) of a Seahorse

260   microplate. The plates were then incubated at 37°C for 2 hours to allow time for the 4T1 cells

261   to adhere. Mitochondrial stress tests were performed per manufacturer's instructions. The OCR

262   was measured as cells were treated sequentially with oligomycin (inhibitor of complex V in the

263   electron transport chain (ETC)), trifluoromethoxy carbonylcyanide phenylhydrazone (FCCP,

264   Sigma-Aldrich, a depolarizer of the mitochondrial membrane potential), and rotenone and

265   antimycin-A (inhibitors of complex I and III in the ETC, respectively). Basal respiration, ATP-

266   linked respiration, and spare capacity were calculated using the Seahorse software.

267

4T1 mouse mammary tumor model

269   The NCI-Frederick Animal Facility, accredited by the Association for Accreditation of Laboratory

270   Animal Care International, follows the Public Health Service Policy for the Care and Use of

271   Laboratory Animals. Animal care was provided in accordance with the procedures outlined in

272   the Guide for Care and Use of Laboratory Animals. Protocols for in vivo studies were approved

273   by the Frederick Animal Care and Use Committee (ACUC). Female BALB/c mice obtained from

274   the Frederick Cancer Research and Development Center Animal Production Area were housed

275   five per cage. Eight to ten-week-old female BALB/c mice were subcutaneously injected with

An *in vitro* tumorigenesis model based on live cell-generated oxygen and nutrient gradients. Gilmore, et al., 2020.

276   2×10^5 4T1 cells. The allograpft tumor volume was measured by Vernier caliper and calculated

277   as volume (mm^3) = (width^2 × length)/2. When the tumors reached 2000 mm^3, typically 30 days

278   post injection, the mice were euthanized, tumors were collected for analysis. Tumors were flash

279   frozen in liquid nitrogen and the tissues were cut into 10 µm thick sections by the

280   Pathology/Histotechnology Laboratory at NCI – Frederick.

281

282   **Fixation**

283   4T1 cells cultured in 12-well plates were fixed in 4% v/v paraformaldehyde for 15 minutes.

284   Samples were rinsed three times in PBS and then blocked and permeabilized in blocking buffer

285   (3% BSA w/v, 0.3% Triton-X100 in 1X DPBS) for 1 hour.

286

287   Fresh frozen sections of 4T1 tumors were fixed in 4% v/v paraformaldehyde for 30 minutes.

288   Samples were rinsed three times in PBS and then blocked and permeabilized in blocking buffer

289   for 1.5 hours.

290

291   **Immunofluorescence Staining**

292   After being fixed, blocked, and permeabilized, cultured 4T1 cells were stained with antibodies

293   diluted in blocking buffer. Incubation times, temperatures, dilutions, and secondaries (if

294   necessary) were used as described in Table 2. For overnight incubations, the samples were kept

295   in a humidified chamber. Cells were then washed three times with 1X PBS and stained with

296   DAPI (300nM; ThermoFisher Scientific) for 15 minutes in 1X PBS. Cells were rinsed an additional

297   three times with 1X PBS prior to storage or imaging.

298

299   After being fixed, blocked, and permeabilized, fresh frozen sections of 4T1 tumors were stained

300   overnight at 4°C with antibodies diluted in blocking buffer, as described in Table 2. Samples

301   were rinsed three times with PBS, stained with DAPI (300nM) for 30 minutes, rinsed again, and

302   sealed for imaging on the Nikon Eclipse Ti widefield fluorescence microscope.

303

304   Table 2:

Antibody & fluorophore	Clone	Vendor – Catalog number	Host	Dilution	Time	Temp.
E-cadherin, direct conjugate (AlexaFluor-488)	24E10	Cell Signaling Technologies – 3199S	Rabbit	1:100	O/N	4°C
Vimentin, direct conjugate (AlexaFluor-555)	D21H3	Cell Signaling Technologies – 9855S	Rabbit	1:50	O/N	4°C
DAPI	NA	ThermoFisher	NA	1:1000	15 min	RT
Nos2, direct conjugate (AlexaFluor-568)	EPR16635	AbCam – 209595	Rabbit	1:100	1 h or O/N	RT 4°C
Cox2, direct conjugate (AlexaFluor-488)	D5H5	Cell Signaling Technologies – 13596S	Rabbit	1:100	1 h or O/N	RT 4°C
HIF1α, direct conjugate (AlexaFluor-647)	EPR16897	AbCam – 208420	Rabbit	1:100	O/N	4°C
ATP5A1 (Mitochondrial ATPase, Primary)	NA	AbClonal – A5884	Rabbit	1:100	O/N	4°C
(Anti-rabbit CF-640R secondary for ATPase)	NA	Biotium – 20178	Donkey	1:100	O/N	4°C
α-Smooth Muscle Actin, direct conjugate (eFluor-488), eBioscience	1A4	ThermoFisher - 41-9760-82	Mouse	1:400	O/N	4°C

An *in vitro* tumorigenesis model based on live cell-generated oxygen and nutrient gradients. Gilmore, et al., 2020.

305

Multiplexed Immunofluorescence

307   After imaging with appropriate filter sets for the directly conjugated antibodies, cell and tissue

308   samples were quenched[26, 27] using a solution comprised of 1 part hydrogen peroxide, 1 part

309   sodium bicarbonate (pH 10) and 3 parts water for 15 minutes at room temperature. Samples

310   were then washed three times with 1X PBS and imaged to ensure quenching. Samples were re-

311   blocked with blocking buffer as described above and re-stained with a new set of directly

312   conjugated antibodies. The quenching cycle can be repeated for at least four rounds of staining

313   without noted damage. DAPI does not quench and can be used to register images for

314   processing. Imaging was performed on the Nikon Eclipse Ti widefield fluorescence microscope.

315

Stimulation of ANA-1 macrophages

317   Murine ANA-1 macrophage cell line was established by infection of normal bone marrow from

318   C57BL/6 mice with J2 recombinant virus[28, 29]. They were cultured in complete media. ANA-1s

319   were stimulated via treatment with IFNγ (100 U/mL) and LPS (20 ng/mL) for 18 to 24 hours. The

320   media was then removed and replaced with fresh stimulation media and subsequent

321   experiments were performed immediately.

322

ANA-1 injection into 4T1 REECs

324   In order to allow time for disks to form, REECs were placed on a 70-80% confluent monolayer of

325   4T1-GFP-luc cells, using the method described above, 3 days prior to ANA-1 injection. ANA-1

326   cells were stimulated with IFNγ and LPS, as described above, 1 day prior to ANA-1 injection. On

327   the day of ANA-1 injection, ANA-1 cells were incubated in serum-free media with CellTracker

328   Red CMTPX Dye (5 µM, ThermoFisher) for at 37 °C for 30 minutes. The ANA-1 cells were then

329   spun down and diluted in complete media (+/- IFNγ and LPS) to ~10,000,000 cells/mL.

330   Immediately prior to injection, the media in the upper chamber of the REECs was refreshed

331   with complete media (+/- IFNγ and LPS). The concentrated ANA-1 solution (10 µL, containing

332   ~100,000 ANA-1 cells) was injected through the opening, directly into the lower chamber of the

333   REEC. For controls, complete media (10 µL, +/- IFNγ and LPS) containing no ANA-1 cells was

334   injected instead. Images were taken every 2 hours for 48 hours on the Nikon Eclipse Ti widefield

335   fluorescence microscope with a 4X dry objective and using a live cell heated stage.

336

337   **Extracellular O_2 concentration quantification in REECs via O_2 sensor foils**

338   To quantify the spatial variation of dissolved $[O_2]$ in the media across the REEC we used O_2

339   sensor foils (PreSens Precision Sensing GmbH, Germany) -- 100 µm thick hydrogels impregnated

340   with particles with $[O_2]$-dependent luminescence. The ratio of the red to blue luminescence

341   correlates with dissolved O_2 concentration. The O_2 sensor foils were glued to the inside top

342   surface of the REEC (made with 200 µm thick stainless-steel washers to maintain a 100 µm

343   chamber height above cells) and a hole was drilled through both the glass and the foil. The

344   response of the sensor foils to $[O_2]$ was calibrated prior to placement on cells using glucose

345   oxidase/catalase solutions of known $[O_2]$ using the Nikon microscope with the 4X objective lens,

346   using the TRITC and DAPI emission filters in rapid succession and exciting the foil with a 395 nm

347   LED lamp. The $[O_2]$ in the glucose oxidase/catalase solution was measured using a Piccolo

348   oxygen sensor system (PyroScience GmbH, Germany). To measure the $[O_2]$ dynamics across the

349   REEC with 4T1 cells in phenol red-free media (1 mL), images of the sensor foil were collected

350   every 15 minutes using the 4X objective lens. A flat-field correction was applied to the images,

351   and the red/blue intensity ratio as a function of distance from the center of the hole was

352   converted via the calibration curve to dissolved $[O_2]$ values (Supplemental Figure 3).

353

354   **Extracellular hypoxia gradient dynamics in REECs via Image-iT Green Hypoxia Reagent**

355   To measure the development of gradients of intracellular hypoxia of live cells in the REECs, cells

356   were incubated with Image-iT Green Hypoxia Reagent (IGHR) (10 µM; Invitrogen) at 37 °C for 30

357   minutes prior to chamber placement. After chamber placement, 4T1 cells were imaged using

358   standard FITC excitation and emission filters at 4X or 20X magnification on a Nikon Eclipse Ti

359   widefield fluorescence microscope. For controls, IGHR treated 4T1 cells were placed in

360   incubators set to 0.1%, 1%, or 5% O_2 or in a standard incubator (~20%) for 2 hours. Cells were

361   immediately imaged (Supplemental Figure 3).

362

363   **Intracellular Hypoxia quantification in REECs**

364   To measure levels of intracellular hypoxia in cell disks, media in the upper chamber was

365   replaced with complete media supplemented with pimonidazole (200 µM; Hypoxyprobe, Inc.,

366   Massachusetts) after disk formation. In hypoxic cells, pimonidazole is reduced and forms

367   adducts with thiol groups. After sufficient time for the pimonidazole to diffuse through the

368   chamber and be taken up by cells (~6 hours), chambers and media were removed, and the disks

369   were immediately fixed, blocked, and permeabilized as described above. A monoclonal

370   antibody specific to pimonidazole adducts and conjugated with a fluorescein probe

371   (Hypoxyprobe-Green Kit (FITC-Mab); Hypoxyprobe, Inc.) was applied for 1 hour at room

372   temperature, or overnight at 4 °C. Samples were rinsed three times with 1X PBS and imaged

373   using standard FITC excitation and emission filters at 20X magnification on the Nikon Eclipse Ti

374   widefield fluorescence microscope. For controls, cultured 4T1 cells were treated with complete

375   media which had been supplemented with pimonidazole and deoxygenated (<1% O_2) with

376   glucose oxidase and catalase. HIF1α expression was determined by immunofluorescence and

377   correlated with pimonidazole adduct formation (Figure 1h).

378

379   **Glucose Gradient dynamics in REECs**

380   2 hours after chamber placement, (2-(N-(7-Nitrobenz-2-oxa-1,3-diazol-4-yl)Amino)-2-

381   Deoxyglucose (2-NBDG) (100 μM; ThermoFisher Scientific) with Hoechst (1 μg/mL) in low-

382   glucose media (5 mM glucose, 10% FBS) was diffused into the chamber for 30 minutes at 37 °C.

383   This dye was often combined with tetramethylrhodamine, ethyl ester (TMRE) (1 nM;

384   ThermoFisher Scientific) in order to obtain simultaneous metabolic measurements. Chambers

385   were removed, rinsed three times in 1X PBS, and imaged using standard excitation and

386   emission filters at 20X on the Nikon Eclipse Ti widefield fluorescence microscope. Samples

387   could be fixed. For measurements in the disk, similar methods were used 7 days after chamber

388   placement on a Zeiss 710 Laser Scanning Confocal Microscope with a 10X dry objective.

389

390   **Live/Dead Staining**

391   4-6 days after chamber placement, media was replaced with media containing the live/dead

392   cell stains ethidium homodimer (2 μM), calcein AM (3 μM), and Hoechst (1 μg/mL;

An *in vitro* tumorigenesis model based on live cell-generated oxygen and nutrient gradients. Gilmore, et al., 2020.

393   ThermoFisher) for 30 minutes. Cells were then imaged on the Nikon Eclipse Ti widefield

394   fluorescence microscope using a live cell heated stage.

395

396   **Celigo Image Acquisition and Analysis**

397   Cells were cultured in 12-well plates with chambers for up to 21 days with weekly media

398   replacement. The plate was scanned using the Cell Counting feature in the Celigo Imaging

399   Cytometer (Nexelom Biosciences) with the brightfield algorithm to detect cells. Cells were

400   segmented using the built-in software.

401

402   **Nos2 and Cox Inhibitor treatments**

403   Immediately prior to chamber placement, the media in each well was replaced with treatment

404   media: complete media supplemented with either the Cox inhibitor indomethacin (100 µM) or

405   the Nos2 inhibitor aminoguanidine (1 mM). Cells were maintained in the REECs for 3-7 days

406   using treatment media before fixation and immunofluorescence staining. For controls, standard

407   complete media was used.

408

409   **Nitric Oxide Production in REECs**

410   4-Amino-5-Methylamino-2',7'-Difluorofluorescein Diacetate (DAF) (ThermoFisher) was used to

411   measure and spatially resolve nitric oxide (NO) production in disks. 7 days after chamber

412   placement, wells were washed three times in 1X PBS to remove all phenol red and BSA, which

413   interfere with DAF fluorescence. To ensure that the lower compartment of the chamber was

414   adequately washed, the 1X PBS was gently pipetted up and down directly over the opening. The

24

415   4T1 cells were then incubated in phenol-red free, serum free media with DAF (10 µM) and

416   Hoechst (µg/mL) at 37 °C for 45 minutes. This dye was often combined with TMRE in order to

417   obtain simultaneous measurements of mitochondrial membrane polarization state. Samples

418   were then immediately imaged on a Zeiss 710 Laser Scanning Confocal Microscope with a 10X

419   dry objective using standard FITC emission and excitation filters.

420

421   **Metabolic Gradient Quantification in REECs**

422   Cells were incubated in phenol red free media with TMRE at 37°C for 20 minutes for cells in

423   standard culture, or 45 minutes for cells in a REEC. TMRE was used simultaneously with 2-NBDG

424   or DAF Diacetate. Cells were imaged with or without chamber removal, depending on the

425   experiment. For controls, the electron transport chain was inhibited with FCCP or antimycin A

426   and rotenone. These treatments caused the TMRE signal to decrease significantly within 15

427   minutes. TMRE was imaged on a Zeiss 710 Laser Scanning Confocal Microscope with a 10X dry

428   objective using Texas Red excitation and emission filters.

429

430   To confirm that mitochondrial mass was consistent across the disk, disks were then fixed,

431   blocked, and permeabilized, as described above. The disks were stained with an ATP-synthase

432   antibody (Abclonal, A5884, Rabbit) diluted 1:100, and incubated at 4°C overnight. Cells were

433   rinsed and incubated with an anti-rabbit secondary at room temperature for 1 hour and then

434   imaged on a Zeiss 710 Laser Scanning Confocal Microscope with a 10X dry objective.

435

436   **Spheroid Growth, Clearing, and Imaging**

437   A spheroid formation assay was performed in ultra-low attachment round bottom 96 well

438   plates (Nexcelom, Lawrence, MA, USA). 4T1 cells or 4T1-GFP-luc cells (for co-culture

439   experiments) were plated in each well (200 µL, 6 x 10^3/mL) with serum-free DMEM

440   supplemented with basic Fibroblast Growth Factor (20 ng/mL) and B-27 supplement (1:50;

441   Thermo Fisher Scientific). Media was supplemented on Day 4. Monoculture spheroids were

442   fixed, cleared, immunolabeled with antibodies and imaged on Day 7 (see below). For coculture

443   experiments, ANA-1 macrophages were stimulated for 18 hours followed by treatment with

444   CellTracker Red CMTPX dye (10µM) at 37°C for 45 minutes and were then added to the

445   spheroids (2 x 10^5 cells/well). The ANA-1-spheroid cocultures were fixed, cleared,

446   immunocytochemically stained with antibodies and imaged on Day 7 (see below).

447

448   Spheroids were cleared for imaging using the Ce3D method[30]. Briefly, spheroids were fixed in

449   4% v/v paraformaldehyde containing 0.5% Triton-X100. Spheroids were blocked at 37°C for 36

450   hours in a humidified environment. Spheroids were then stained with directly conjugated

451   antibodies for proteins of interest (HIF1α, Nos2, Cox2) at 4 °C for 36 hours. Spheroids were

452   stained with DAPI (300 nM) for 30 minutes and then rinsed three times with 1X PBS. The

453   spheroids were then embedded in 1.5% low-melt agarose. Samples were placed in clearing

454   solution (0.1% v/v Triton-X100, 13% N-methylacetamide, 66% w/v Nycodenz AG) at room

455   temperature for 4 hours at a 1:4 agarose:clearing solution ratio. After 4 hours, the clearing

456   solution was replaced with the equivalent volume of fresh clearing solution and left overnight.

457

458   The cleared spheroids were imaged on a Leica TCS SP8 Laser Scanning Confocal microscope at

459   20X with oil to match the index of refraction of the clearing solution (slightly higher than 1.5). Z-

460   stacks were taken through the center of the spheroids.

461

462   **Image Processing and Data Analysis**

463   Images taken on the Nikon Eclipse Ti widefield fluorescence microscope were typically stitched

464   and background corrected using a rolling ball technique in Nikon Elements software, then

465   processed in Imaris (Bitplane). Image brightness and contrast were adjusted to optimize the

466   visual dynamic range for display. Imaris was used for cell segmentation and to extract position,

467   fluorescence intensity, and geometrical statistics on each cell. Custom R scripts were used to

468   process the output of Imaris statistics, including average cell intensity for each channel and

469   position. For cell disks, cells were binned into annuli every 50 µm from the center, and the

470   mean fluorescence intensity (MFI) per cell in that bin was calculated. Disks that could not be

471   segmented were analyzed in FIJI using the Radial Profile plug-in, which averages the intensity

472   value of all pixels at each radius from a fixed point. For the spheroid and tissue images, custom

473   MATLAB functions were used to calculate fluorescence intensity and depth (spheroid) or

474   position (tissue) for each pixel and averaged as above. For disks and spheroids intensity profiles,

475   R scripts were used to average those radial mean values within 50 µm wide annuli. For cell

476   disks, radial values were normalized to disk radius, and MFI were normalized to the value at r =

477   0 for that disk or the control group disk. For the NBDG/TMRE data, MFI were normalized to the

478   maximum MFI value for each profile, and the normalized curves were averaged. For spheroids,

479   depth values were normalized to the maximum depth of each spheroid (such that 0 represents

480   the surface and 1 is the maximum depth), and MFI were normalized to the value at the

481   spheroid surface. For tissue, MFI was normalized to the first position in the profile. All data are

482   presented as mean +/- SEM unless otherwise noted. Statistical significance, determined using

483   Welch's two-tailed t-test, and Pearson correlation coefficients were calculated in GraphPad

484   Prism and Microsoft Excel.

485   ## Data Availability

486   The data that support the findings of this study are available from the corresponding author

487   upon request.

488   ## Code Availability

489   The code supporting the plots and other findings in the manuscript are available from the

490   corresponding author upon request.

491   ## References

492   1.   Petrova, V., Annicchiarico-Petruzzelli, M., Melino, G. & Amelio, I. The hypoxic tumour

493   microenvironment. *Oncogenesis* **7** (2018).

494   2.   Byrne, M.B., Leslie, M.T., Gaskins, H.R. & Kenis, P.J.A. Methods to study the tumor

495   microenvironment under controlled oxygen conditions. *Trends in Biotechnology* **32**, 556-

496   563 (2014).

497   3.   Keenan, T.M. & Folch, A. Biomolecular gradients in cell culture systems. *Lab on a Chip* **8**,

498   34-57 (2007).

499   4.   Friedrich, J., Seidel, C., Ebner, R. & Kunz-Schughart, L.A. Spheroid-based drug screen:

500   Considerations and practical approach. *Nature Protocols* (2009).

501   5.   Nath, S. & Devi, G.R. Three-dimensional culture systems in cancer research: Focus on

502   tumor spheroid model. *Pharmacology and Therapeutics* **163**, 94-108 (2016).

503   6.   Hoh, J.H., Werbin, J.L. & Heinz, W.F. Restricted exchange microenvironments for cell

504   culture. *BioTechniques* **64**, 1-6 (2018).

505   7.   Pulaski, B.A. & Ostrand-Rosenberg, S. Mouse 4T1 Breast Tumor Model. *Current*

506   *Protocols in Immunology* **39**, 20.22.21-20.22.16 (2000).

507   8.   Noy, R. & Pollard, Jeffrey W. Tumor-Associated Macrophages: From Mechanisms to

508   Therapy. *Immunity* **41**, 49-61 (2014).

509   9.   Lehmann, S. et al. Hypoxia Induces a HIF-1-Dependent Transition from Collective-to-

510   Amoeboid Dissemination in Epithelial Cancer Cells. *Current Biology* (2017).

511   10.   Nieto, M.A., Huang, R.Y.-j., Jackson, R.A. & Thiery, J.P. Review EMT : 2016. *Cell* **166**, 21-

512   45 (2016).

513   11.   Basudhar, D. et al. Coexpression of NOS2 and COX2 accelerates tumor growth and

514   reduces survival in estrogen receptor-negative breast cancer. *Proceedings of the*

515   *National Academy of Sciences* **114**, 13030-13035 (2017).

516   12.   Somasundaram, V. et al. Molecular Mechanisms of Nitric Oxide in Cancer Progression,

517   Signal Transduction, and Metabolism. *Antioxidants & Redox Signaling* **30**, 1124-1143

518   (2018).

519   13.   Heinecke, J.L. et al. Tumor microenvironment-based feed-forward regulation of NOS2 in

520   breast cancer progression. *Proc Natl Acad Sci U S A* **111**, 6323-6328 (2014).

521   14.   Basudhar, D. et al. Understanding the tumour micro-environment communication

522   network from an NOS2/COX2 perspective. *Br J Pharmacol* **176**, 155-176 (2019).

523   15.   Somasundaram, V. et al. Inducible nitric oxide synthase-derived extracellular nitric oxide

524   flux regulates proinflammatory responses at the single cell level. *Redox Biology* **28**,

525   101354 (2020).

526   16.   Olson, N. & Van Der Vliet, A. Interactions between nitric oxide and hypoxia-inducible

527   factor signaling pathways in inflammatory disease. *Nitric Oxide - Biology and Chemistry*

528   **25**, 125-137 (2011).

529   17.   Cyr, A. et al. Endotoxin Engages Mitochondrial Quality Control via an iNOS-Reactive

530   Oxygen Species Signaling Pathway in Hepatocytes. *Oxid Med Cell Longev* **2019**, 4745067

531   (2019).

532   18.   Vitale, I., Manic, G., Coussens, L.M., Kroemer, G. & Galluzzi, L. Macrophages and

533   Metabolism in the Tumor Microenvironment. *Cell Metab* **30**, 36-50 (2019).

534   19.   Jeong, S.K. et al. Tumor associated macrophages provide the survival resistance of

535   tumor cells to hypoxic microenvironmental condition through IL-6 receptor-mediated

536   signals. *Immunobiology* **222**, 55-65 (2017).

537   20.   Oyler-Yaniv, A. et al. A Tunable Diffusion-Consumption Mechanism of Cytokine

538   Propagation Enables Plasticity in Cell-to-Cell Communication in the Immune System.

539   *Immunity* **46**, 609-620 (2017).

540   21.   Pettersen, E.O., Larsen, L.H., Ramsing, N.B. & Ebbesen, P. Pericellular oxygen depletion

541   during ordinary tissue culturing measured with oxygen microsensors. *Cell Proliferation*

542   **38**, 257-267 (2005).

543   22.   Suhaimi, H., Wang, S. & Das, D.B. Glucose diffusivity in cell culture medium. *Chemical*

544   *Engineering Journal* **269**, 323-327 (2015).

545   23.   Simões, R.V. et al. Metabolic Plasticity of Metastatic Breast Cancer Cells: Adaptation to

546   Changes in the Microenvironment. *Neoplasia* **17**, 671-684 (2015).

547   24.   Wenger, R., Kurtcuoglu, V., Scholz, C., Marti, H. & Hoogewijs, D. Frequently asked

548   questions in hypoxia research. *Hypoxia* **3**, 35 (2015).

549   25.   Al-Ani, A. et al. Oxygenation in cell culture: Critical parameters for reproducibility are

550   routinely not reported. *PLoS One* **13**, e0204269 (2018).

551   26.   Gerdes, M.J. et al. Highly multiplexed single-cell analysis of formalin-fixed, paraffin-

552   embedded cancer tissue. *Proceedings of the National Academy of Sciences* **110**, 11982-

553   11987 (2013).

554   27.   Lin, J.R., Fallahi-Sichani, M., Chen, J.Y. & Sorger, P.K. Cyclic Immunofluorescence (CycIF),

555   A Highly Multiplexed Method for Single-cell Imaging. *Current protocols in chemical*

556   *biology* **8**, 251-264 (2016).

557   28.   Blasi, E., Radzioch, D., Durum, S.K. & Varesio, L. A murine macrophage cell line,

558   immortalized by v-raf and v-myc oncogenes, exhibits normal macrophage functions. *Eur*

559   *J Immunol* **17**, 1491-1498 (1987).

560   29.   Blasi, E. et al. Selective immortalization of murine macrophages from fresh bone

561   marrow by a raf/myc recombinant murine retrovirus. *Nature* **318**, 667-670 (1985).

562   30.   Li, W., Germain, R.N. & Gerner, M.Y. Multiplex , quantitative cellular analysis in large

563   tissue volumes with clearing-enhanced 3D microscopy (C e 3D). *Proceedings of the*

564   *National Academy of Sciences* (2017).

An *in vitro* tumorigenesis model based on live cell-generated oxygen and nutrient gradients. Gilmore, et al., 2020.

Acknowledgments

Author contributions

WFH, SJL, and DAW conceived the project, and ACG, SJF, VS, and WFH designed the experiments. ACG and SJF constructed the REECs, performed all experiments with the chambers, wrote analysis software, and processed and analyzed the images. VS grew the spheroids and performed the mouse experiments and assisted ACG with the Seahorse measurements. ACG imaged the spheroids and tissue samples. DAS assisted with multiplexed immunofluorescence imaging and image analysis. WFH implemented the mathematical model. ACG, SJF, and WFH wrote the manuscript, and all authors critically reviewed the manuscript.

Ethics declarations

Competing interests

The authors declare no competing interests